BIROn - Birkbeck Institutional Research Online

Using stable Mg isotope signatures to assess the fate of magnesium during the *in situ* mineralisation of CO_2 and H_2S at the CarbFix site in SW-Iceland

Eric H. Oelkers[1,2,3], Rhiannon Butcher[3], Philip A.E. Pogge von Strandmann[3], Jan A. Schuessler[4], Friedhelm von Blankenburg[4], Sandra Ó. Snæbjörnsdóttir[1,5], Kiflom Mesfin[1], Edda Sif Aradóttir[5], Ingvi Gunnarsson[5], Bergur Sigfússon [5], Einar Gunnlaugsson[5], Juerg M. Matter[6,7], Martin Stute[7], Sigurdur R. Gislason[1]

[1]*Institute of Earth Science, University of Iceland, Iceland*
[2]*CNRS/UMR 5563, Université Paul Sabatier, France*
[3]*London Geochemistry and Isotope Centre (LOGIC), University College London and Birkbeck, University of London, Gower Place, London, UK.*
[4]*GFZ German Research Centre for Geosciences, Telegrafenberg, 14473 Potsdam, Germany*
[5]*Reykjavik Energy, Iceland*
[6]*Ocean and Earth Science, University of Southampton, UK*
[7]*Lamont-Doherty Earth Observatory, Columbia University, USA*

Abstract - The *in-situ* carbonation of basaltic rocks could provide a long-term carbon storage solution. To investigate the viability of this carbon storage solution, 175 tonnes of pure CO_2 and 73 tonnes of a 75% CO_2-24% H_2S-1% H_2-gas mixture were sequentially injected into basaltic rocks as a dissolved aqueous fluid at the CarbFix site at Hellisheidi, SW-Iceland. This paper reports the Mg stable isotope compositions of sub-surface fluids sampled prior to, during, and after the CO_2 injections. These Mg isotopic compositions are used to trace the fate of this element during the subsurface carbonation of basalts. The measured Mg isotopic compositions of the monitoring well fluids are isotopically lighter than the dissolving basalts and continue to become increasingly lighter for at least two years after the gas-charged water injection was stopped. The results indicate that the formation of isotopically heavy Mg-clays rather than Mg-carbonates are the predominant Mg secondary phases precipitating from the sampled fluids. Isotope mass balance calculations suggest that more than 70% of the Mg liberated from the basalt by the injected gas charged water was precipitated as Mg-clays, with this percentage increasing with time after the injection, consistent with the continued precipitation of Mg clays over

38   the whole of the study period. The formation of Mg clays in response to the injection of
39   CO_2 into basalts, as indicated in this study, could be detrimental to carbon storage efforts
40   because the formation of these minerals consume divalent Mg that could otherwise be
41   used for the formation of carbonate minerals and because such clays could decrease host
42   rock permeability.

43

44   **1. Introduction**

45   The CarbFix project was created to develop the technology to store carbon dioxide as
46   stable carbonate minerals directly in the subsurface by reacting gas charged injection
47   waters with basaltic rocks (Gislason et al., 2010, 2018; Aradóttir et al., 2011, 2018).
48   Carbon storage in basaltic rocks offers numerous advantages including their ability to
49   promote mineral carbonation and their large potential storage volume (McGrail et al.,
50   2006; Goldberg and Slagle, 2009; Goldberg et al., 2010; Gislason and Oelkers, 2014;
51   Snæbjörnsdóttir et al., 2014). As such, numerous studies have focused on developing the
52   technology to safely store CO_2 in basaltic rocks including laboratory (Assayag et al.,
53   2009; Flaathen et al., 2009; Gudbrandsson et al., 2011; Stockmann et al., 2011; Gysi and
54   Stefánsson, 2012; Rosenbauer et al., 2012; Galeczka et al., 2014; Mareni et al., 2018),
55   modelling (McGrail et al., 2006; Van Pham et al., 2012; Goldberg et al., 2009, 2013;
56   Rosenbauer et al., 2012; Bacon et al., 2014) and field efforts (Rogers et al., 2006; Matter
57   et al., 2007; McGrail et al., 2011, 2012; Siggfusson et al., 2015). Basaltic rocks are rich in
58   divalent cations such as Ca^{2+}, Mg^{2+}, and Fe^{2+}. The injection of acidic CO_2-charged water
59   promotes the release of these metals, potentially leading to the formation of carbonate
60   minerals such as calcite, magnesite, and siderite as the continued dissolution of basalt
61   increases the pH of the aqueous fluid (Oelkers et al., 2008; Gislason et al., 2010, 2014;
62   Stefánsson et al., 2011; Gislason and Oelkers, 2014; Olsson et al., 2014). About 5% of
63   the continents and most of the oceanic floor are comprised of basaltic rocks, including the
64   mid-oceanic ridges. As such the largest basaltic storage potential lies offshore;
65   theoretically all CO_2 from the burning of fossil fuel carbon (estimated to be ~5000 Gt;
66   Archer, 2005) could be stored by mineral carbonation along the mid-ocean ridges
67   (Snæbjörnsdóttir et al., 2014). The flanks of these ridges contain highly fractured and
68   permeable basaltic layers (Fisher, 1998) with a pervasive circulation of about 1,000 Gt

69   seawater/yr (Harris and Chapman, 2004). The potential for using these marine systems

70   for carbon storage is confirmed by the results of Wolff-Boenisch et al. (2011), who

71   demonstrated the rapid dissolution of basaltic rocks in CO_2 charged seawater.

72

73   The efficiency of mineral carbonation, however, can be limited if Mg clay minerals

74   rather than Mg carbonate minerals form in response to the injection of CO_2 into basalts.

75   Magnesium clay formation is detrimental to carbon storage efforts because these minerals

76   consume divalent Mg that could otherwise be used for the carbonate mineral formation,

77   and because Mg-bearing clays could decrease host rock permeability. The fate of Mg

78   during mineral carbonation efforts in basalts will be assessed in this study through the

79   application of Mg isotopes. The stable isotopes of magnesium (^{24}Mg, ^{25}Mg and ^{26}Mg)

80   are increasingly being used as tracers of geochemical processes, including their use to

81   assess mineral reactions during weathering (Brenot et al., 2008; Huang et al., 2012; Liu et

82   al., 2014; Pogge von Strandmann et al., 2012; Tipper et al., 2006, 2008, 2012a, 2012b;

83   Wimpenny et al., 2011). Like all major elements, magnesium and its isotopes are affected

84   by a number of processes. For example, the magnitude and sign of Mg isotope

85   fractionation during precipitation appears to be dependent on the type of mineral forming

86   (Geske et al., 2012; 2015; Immenhauser et al., 2010; Li et al., 2012, 2015; Saulnier et al.,

87   2012; Wombacher et al., 2011), organic vs. inorganic precipitation (Chang et al., 2004;

88   Pogge von Strandmann, 2008; Saenger and Wang, 2014), precipitation rate (Mavromatis

89   et al., 2013), fractionation mechanism (Buhl et al., 2007), and aqueous speciation (Li et

90   al., 2014; Schott et al., 2016). In addition, isotopic fractionation can also occur due to

91   both the preferential incorporation and preferential adsorption of specific Mg isotopes

92   (Huang et al., 2012; Liu et al., 2014; Opfergelt et al., 2011; Pogge von Strandmann et al.,

93   2008, 2012; Tipper et al., 2012a; Wimpenny et al., 2010, 2014). Finally, the uptake of

94   Mg by plants and microbes causes variable isotope fractionation (Black et al., 2006;

95   Bolou-Bi et al., 2010, 2012; Oelkers et al., 2015; Pokharel et al., 2017; Uhlig et al.,

96   2017).

97

98   In this study the Mg isotope systematics of subsurface fluids sampled prior to, during,

99   and after the injection of CO_2-charged waters into subsurface basalts was measured to

100 provide insight into the mineralisation reactions that occurred in response to this
101 injection. This approach takes advantage of the distinct Mg isotope fractionation
102 signatures of primary and secondary phases. The Mg isotope ratio of primary igneous
103 silicate rocks is virtually uniform (Teng et al., 2010a; Pogge von Strandmann et al., 2011)
104 and it differs markedly from that in carbonates (Chang et al., 2004; Pogge von
105 Strandmann, 2008; Wombacher et al., 2011; Li et al., 2012, 2014; Saenger and Wang,
106 2014, Teng 2017). As such, the Mg isotope composition of surface waters is often
107 controlled by the balance of dissolution of silicate to carbonate rocks in the host
108 catchment and/or the relative precipitation rates of Mg-clays compared to Mg-bearing
109 carbonates (Tipper et al., 2006a, 2006b, 2008; Pogge von Strandmann et al., 2008, 2014).
110 It is thus anticipated that a similar approach will provide insight into the identity of Mg
111 minerals formed during subsurface processes occurring at the CarbFix site.

112
113

2. Background of the CarbFix Project

115 This study focuses on the fate of Mg liberated from dissolving basalts in response to
116 the injection of CO_2-charged water at the CarbFix injection site. A number of past
117 publications have reported the details of this injection, including the temporal evolution
118 of dissolved element compositions and chemical tracers following these injections. A
119 description of the injection method was presented by Sigfússon et al. (2015). The
120 temporal evolution of chemical tracers, dissolved carbon and pH in the first monitoring
121 well downstream from the injection well was reported by Matter et al. (2016), as well as
122 an estimate of the fraction of injected carbon fixed by carbonation reactions. This study
123 concluded that more than 95% of the dissolved carbon injected into the subsurface was
124 fixed as stable carbonate minerals within 2 years. The concentrations of dissolved major
125 elements during and after injection in the first monitoring well, as well as the saturation
126 indices of potential secondary minerals were described by Snæbjörnsdóttir et al. (2017).
127 Reaction path modelling of the carbon dioxide charged injection fluids, as they reacted
128 with the subsurface basalts were reported by Snæbjörnsdóttir et al. (2018).

129

130 The CarbFix injection site is equipped with a 2000 m deep injection well and 8

131   monitoring wells ranging in depth from 50 to 1300 m in depth. The subsurface rocks at
132   the injection site are primarily olivine tholeiite basalts consisting of lava flows and
133   hyaloclastite formations (see Fig. 1). The hyaloclastites are relatively low permeability
134   glassy rocks formed under ice and melt water during glaciations; the boundaries between
135   hyaloclastites and lava flows, and those between individual lava flows boundaries are
136   preferential fluid flow pathways (Alfredsson et al., 2013). Some alteration is observed in
137   the hyaloclastite rocks starting at 120 to 300 m depth. The common alteration minerals at
138   this depth are smectite, calcite, Ca-rich zeolites, and poorly crystalline iron-hydroxides
139   (Alfredsson et al., 2013). Fluid injection was targeted at a lava flow sequence located
140   400–800 m below the surface with the main aquifer located at ~530 m depth. Loss on
141   ignition measurements on rock samples suggest that over 80% of the primary rocks in the
142   target zone are currently unaltered. Tracer tests were conducted both under natural and
143   forced flow conditions from 2008 to 2011 to define the system hydrology (Aradóttir et
144   al., 2012; Gislason et al., 2010; Khalilabad et al., 2008). These tests indicated that the
145   flow from the HN-02 injection well to the first monitoring well (HN-04) consists of
146   relatively homogenous porous media intersected by a low volume and fast flow path that
147   channels about 3% of the tracer flow (Khalilabad et al., 2008).

148

149   The water in the target zone prior to the injection ranged in temperature from 15 to 35
150   °C and had *in situ* pH ranging from 8.4 to 9.8. The concentrations of dissolved CO_2 and
151   O_2 collected from the injection well from the target reservoir were 1.27 x10^{-3} and 1.1x10^{-5}
152   mol/kg, respectively, prior to the injection (Alfredsson et al., 2013). These values are
153   substantially undersaturated with respect to the composition of these gases in the
154   atmosphere, suggesting that the target injection reservoir was isolated from the surface.
155   The concentration of Ca and Mg in these waters prior to the injection was limited by
156   secondary mineral precipitation (Alfredsson et al., 2013). All the water samples collected
157   from the target reservoir prior to the injection of CO_2 charged water were supersaturated
158   with respect to Ca-zeolite, analcime, Ca–Mg–Fe smectite, calcite, and aragonite, and
159   some are supersaturated with respect to dolomite and Fe–Mg carbonates (Snæbjörnsdóttir
160   et al., 2017).

161

Approximately 175 tons of pure commercial CO_2 and 73 tons of a 75%–24%–0.8% mixture of CO_2–H_2S–H_2 gases were dissolved into water during their injection from January until August 2012. This latter gas mixture was captured directly from the adjoining Hellisheidi power plant by its dissolution into water at elevated pressure (Gislason et al., 2018; Sigfusson et al., 2018). The injected water had a temperature of ~25 °C and was equilibrated with 26 to 28 bars pressure of the CO_2 gas or ~14 bars pressure of the CO_2–H_2S–H_2 mixture. The injected fluid equilibrated with pure carbon dioxide had dissolved CO_2 concentrations of ~0.8 mol/kg H_2O and a pH of 3.85, whereas the fluid equilibrated with the gas mixture had a dissolved CO_2 concentration of ~0.43 mol/kg H_2O and a pH of 4.0 (Snæbjörnsdóttir et al., 2017). All host rock minerals and glass were strongly undersaturated with respect to the gas charged injection waters (Snæbjörnsdóttir et al., 2018). The interaction of these acidic fluids with the host basalts creates porosity near the injection well by dissolving primary and secondary minerals. As gas-charged water continues to dissolve the basaltic host rock, this fluid becomes increasingly basic and secondary minerals will precipitate, potentially clogging the system. Reaction path calculations reported by Snæbjörnsdóttir et al. (2018) suggested that Mg–Fe–carbonates and siderite became supersaturated in the subsurface fluids at pH <5, whereas Ca-Mg-Fe-carbonates and calcite were saturated or supersaturated at higher pH. Mg bearing clays and Ca, Na-rich zeolites also became saturated in the subsurface fluids at pH >7.

182

3. Sampling and Analytical Methods

A detailed overview of fluid injection and sampling before, during and after the CarbFix injections have been reported by Snæbjörnsdóttir et al. (2017). Sampling of the fluids from the HN-04 monitoring well and other wells surrounding the injection well began in 2008. Water samples for chemical analysis were collected several times prior to the injections, which began during January 2012 (Alfredsson et al., 2013). During the injections and until mid-September 2012 the HN-04 injection well was sampled twice weekly. Weekly sampling continued until mid-July 2013 with few exceptions. Water was

191   pumped from this monitoring well at the rate of 3.5 m^3/h throughout this study

192   maintaining a constant head from the injection to the monitoring well.

193

194   Fluid samples were collected via a 10 m long, 10 mm diameter stainless steel pipe

195   connected to the 53 mm diameter monitoring well lining pipe extending down to the

196   pump (Alfredsson et al., 2016). The sample pipe was connected directly to a sampling

197   valve inside an on-site field laboratory. After flushing the sampling pipe, the sampled

198   waters were immediately filtered through 0.2 μm Millipore cellulose acetate membranes

199   using silicon tubing and a 140 mm Sartorius® filter holder. All air in the filtration system

200   was expelled through a valve prior to sampling and at least 3 L of water was pumped

201   through the system before the samples were collected in acid washed high density

202   polyethylene bottles for cation and isotopic analysis. The sampling bottles were also

203   washed with the monitoring well fluids three times before the final sampling. These

204   samples were acidified using Suprapur® HNO$_3$, 1% (v/v) then stored prior to analysis.

205   The fluid sample Si, Ca, Mg concentrations, alkalinity and pH data used in this study

206   were previously reported by Snæbjörnsdóttir et al. (2017) and Alfredsson et al. (2013).

207   Four pre-CO$_2$-injection fluid samples from different shallow wells and 19 post-injection

208   monitoring well (HN-04) samples were selected for Mg isotope measurements (Table 1).

209   Samples collected prior to the acid gas injections from the deep wells (> 400 m),

210   including the HN-04 monitoring well, could not be analysed for their Mg isotopic ratios

211   due to their low Mg concentrations (see Fig. 2). These concentrations did not exceed 6

212   μmol kg^{-1}(Alfredsson et al., 2013; Snæbjörnsdóttir, et al., 2017).

213

214   ***Mg isotope analyses***   - Prior to stable Mg isotope analyses, the fluid samples were

215   chemically purified by cation exchange chromatography in a clean laboratory equipped

216   with filtered air laminar flow workstations at GET Toulouse following a protocol similar

217   to that reported by Mavromatis et al. (2012, 2013), Pearce et al. (2012), and Shirokova et

218   al. (2013). Briefly, fluid samples were evaporated to dryness and re-dissolved in 1M

219   HNO$_3$ prior to loading onto 10 ml Bio-Rad poly-prop columns containing AG-50W-X12

220   resin (200–400 mesh) for separation of Mg from other elements. A total of 23 samples

221   were processed in two batches of Mg column chemistry. With each batch of samples, the

222 IAPSO seawater reference material and a procedure blank was processed for quality
223 control. Mg recovery after chromatographic separation was >99.5%. After column
224 chemistry, samples were evaporated, treated with H_2O_2/HNO_3 at 150°C to remove any
225 remaining organics, and finally re-dissolved in 0.3M HNO_3.

226

227   Mg isotope measurements were performed at the HELGES lab, GFZ Potsdam,
228 following protocols described by Uhlig et al. (2017) and Pokharel et al. (2017). Before
229 Mg isotope ratio analysis, the purity of the Mg sample solutions and the Mg content in
230 procedure blanks were checked by ICP-OES (Varian 720ES) and quadrupole ICP-MS
231 (Thermo iCAP-Qc), respectively. Most of the samples showed a purity of higher than
232 99% Mg; for some samples that did not, we tested that the remaining impurities of Na
233 and K would cause no analytical bias. Doping DSM-3 with Na and K and measuring the
234 Mg isotopic composition showed that the impurities did not bias the Mg isotope
235 measurements, i.e., the Na-K-doped DSM-3 ($\delta^{26}Mg$ = -0.05±0.10 ‰, 2SD) was identical
236 to pure DSM-3 within analytical uncertainty, consistent with previous findings (Pokharel
237 et al., 2017). Procedural blanks contributed less than 0.9% to the Mg processed through
238 column chemistry (15 µg) and are therefore considered insignificant (potential bias in
239 $\delta^{26}Mg$ is less than 0.04 ‰). All Mg isotope ratio measurements were performed in
240 medium resolution mode on a Thermo Neptune multi-collector inductively coupled
241 plasma mass spectrometer (MC-ICP-MS). Samples and the DSM3 bracketing standard
242 were diluted in 0.3 M HNO_3 to 500 ppb. The solutions were introduced to the MC-ICP-
243 MS via a quartz-glass spray chamber (double pass cyclon-scott type, Thermo SIS)
244 equipped with a self-aspirating ca. 100 µL/min. The Mg isotope signals ($^{24}Mg^+$, $^{25}Mg^+$,
245 $^{26}Mg^+$) were measured simultaneously on Faraday detectors. ^{26}Mg was measured on the
246 interference-free low mass side of the flat-top peak to avoid interference from $^{12}C^{14}N^+$.
247 Sample signal intensities of ca. 12 V for $^{24}Mg^+$ were obtained. Background intensities (<
248 8 mV $^{24}Mg^+$) were measured on-peak in 0.3 M HNO_3 before and after each sample
249 measurement block and were subtracted from sample signal intensities. Instrumental
250 mass bias on measured Mg isotope ratios was corrected by the sample-standard
251 bracketing method using concentration-matched DSM3 as a standard.

252

253   We report isotope ratios of samples as per mil deviation of the ^{26}Mg/^{24}Mg and

254   ^{25}Mg/^{24}Mg ratios from the DSM3 international reference material using the delta

255   notation, as δ^{26}Mg and δ^{25}Mg, respectively. All results are consistent with mass

256   dependent isotope fractionation. Average δ-values obtained from 2 to 6 replicate

257   measurements of the same fluid are reported in Table 1 together with twice the standard

258   deviation (2SD), which indicates the instrument repeatability. To assess total analysis

259   uncertainty, IAPSO Atlantic seawater was also analysed with our samples and gave a

260   mean δ^{26}Mg of -0.90±0.08 (n = 12), which is in agreement with literature reference values

261   (-0.83 ±0.09 ‰, 2SD, Foster et al. 2010, Ling et al. 2011 and references therein). The

262   pure Mg solution Cambridge-1 was measured 21 times during this study and gave a δ^{26}Mg

263   of -2.62±0.10‰ (2SD), which is also in close agreement with literature values (-2.59 to

264   2.78‰ – see compilations by Pogge von Strandmann et al., 2011; An and Huang, 2014).

265   These observations are consistent with previously established long-term uncertainty

266   estimates of the MC-ICP-MS method at GFZ HELGES of ±0.06‰ (2SD) for δ^{25}Mg and

267   ±0.10‰ (2SD) for δ^{26}Mg (Uhlig et al., 2017; Pokharel et al., 2017).

268

4. Results

270   The Mg isotope compositions of four pre-injection shallow well samples,

271   collected during 2008 and 2010 from wells HK-12, HK-13, and HK-25, which are drilled

272   to depths of 130, 210 and 310 m, respectively, are shown in Fig. 3, and listed in Table 1;

273   the composition of selected elements in these fluids are provided in Table 2. The

274   measured δ^{26}Mg of these samples ranged from -0.57 to -0.69 ‰, which is ~0.3‰ lower

275   than basaltic rocks from this area and previously measured groundwaters in Iceland

276   (Pogge von Strandmann et al., 2008), but within the range of precipitation-uncorrected

277   Icelandic soil pore waters (Pogge von Strandmann et al., 2012). Note that the formation

278   of Mg-bearing clays in these systems occurs only at depths greater that 120 to 300 m

279   (Alfredsson et al., 2013), such that these shallow water samples are likely relatively

280   unaffected by Mg clay precipitation compared to deeper wells, which is also consistent

281   with the relatively high Mg concentrations of these fluids.

282

283   The fluid compositions of the HN-04 monitoring well fluids are provided in Tables
284   1 and 2. The first of these samples analysed for δ^{26}Mg was collected on 9 February 2012,
285   17 days after the start of the initial CO_2-charged water injection. This sample had a Mg
286   concentration of 36 μmol kg^{-1} and a δ^{26}Mg of -0.84 ‰, which is approximately 0.25 ‰
287   lower than that of the pre-injection shallow well samples. As the aqueous Mg
288   concentrations of the monitoring well fluids increased with time up to 101 μmol kg^{-1} on
289   26 March 2012 (Fig. 2b) the δ^{26}Mg values of these fluids decreased to -0.94 ‰. These
290   δ^{26}Mg values continued to decrease with time to about -1.3 ‰ through June 2013 as the
291   dissolved Mg concentration decreased, increased, and decreased again in response to the
292   arrival to the monitoring well of fluids influenced by the injection of the acid gases (see
293   Fig. 2, 3). The isotopically lightest δ^{26}Mg value of -1.34 ‰ was measured in the final
294   sample collected on 8 June 2014.

295

296   **5. Discussion**

297   The basaltic glass in the region of CarbFix injection site has a δ^{26}Mg value
298   of -0.28‰ (Pogge von Strandmann et al., 2008; Wimpenny et al., 2010), which is
299   identical to State University of New York (SUNY) Mid-Ocean Ridge Basalt (MORB;
300   Teng et al., 2007), as well as the bulk silicate Earth (Hin et al., 2017). This glass is
301   susceptible to dissolution in response to the injection of acidic fluids (Gislason et al,
302   1996; Oelkers, 2001; Oelkers and Gislason, 2001; Gislason and Oelkers, 2003) and has
303   been identified as the major phase dissolving in response to the CarbFix gas charged
304   water injections (Snæbjörnsdóttir et al., 2018). The rapid fluid-flow pathway, channeling
305   ~3% of the injected gas charged fluid was attributed to a fracture network located in
306   crystalline basalts containing mainly plagioclase, olivine, and pyroxene. Nevertheless
307   olivines and crystalline basalts near the CarbFix site have an identical δ^{26}Mg composition
308   to each other and the basaltic glass (Pogge von Strandmann et al., 2008, 2012). This is
309   consistent with other studies suggesting basaltic olivines have a narrow isotopic range,
310   with a similar Mg isotope composition to that of its coexisting basalt glass (Norman et
311   al., 2006; Teng et al., 2007; Wimpenny et al., 2010; Liu et al., 2017). Although such
312   results indicate that the preferential dissolution of distinct primary phases will not cause
313   significant Mg isotope fractionation, it should be noted that both Wimpenny et al. (2010)

314 and Maher et al. (2016) reported an initial preferential loss of light Mg during the
315 dissolution of basaltic glass and olivine. Longer-term experiments reported by Oelkers et
316 al. (2015) however, suggest that for the case of olivine, this preferential release of light
317 Mg is limited to the initial stages of dissolution.

318

319   The low Mg concentrations in the target reservoir fluids prior to the gas injection
320 indicate that essentially all the Mg dissolved in the HN-04 monitoring well samples
321 collected in this study after January 2012 originates from the injected fluids or the
322 dissolution of the host minerals in response to fluid-rock interaction. The low Mg
323 concentrations of the target reservoir prior to injection have been attributed to the
324 formation of Mg-bearing secondary minerals in the subsurface reservoirs, and in
325 particular to Mg-bearing clay precipitation. Indeed, the smectite, Mg-saponite, is
326 calculated to be strongly supersaturated in these fluids prior to injection, whereas
327 dolomite and magnesite are undersaturated (Snæbjörnsdóttir, et al., 2017). These
328 calculated results are consistent with the observed secondary minerals in the target basalt
329 formations (Alfredsson et al., 2013). They also explain the low δ^{26}Mg of the pre-injection
330 shallow reservoir fluids compared to that of the host basalt, as Mg-bearing silicate
331 minerals preferentially incorporate heavy Mg isotopes upon their formation (c.f. Young
332 and Galy, 2004; Tipper et al., 2006; Teng et al., 2007, 2010; Pogge von Strandmann et
333 al., 2008).

334

335   It seems likely, therefore, that the increasingly isotopically light composition of
336 the post-injection well samples must either be caused by continued dissolution of an
337 isotopically light and previously formed secondary phase, or the precipitation of an
338 isotopically heavy secondary phase. Evidence suggests the calcite present in the host
339 basalts dissolve as the acidic gas charged injection waters first interact with the
340 subsurface basalts (Snæbjörnsdóttir et al., 2017). This calcite likely has a δ^{26}Mg of no
341 more than -1.4‰ (Saenger and Wang 2014; Wombacher et al., 2011) such that the initial
342 dissolution of calcite would tend to make the fluids lighter. Nevertheless, after a short
343 initial time, saturation state and reactive path calculations indicate that calcite, as well as
344 dolomite and mixed Mg-Ca-Fe carbonates, become supersaturated in the monitoring

345   fluids collected from the HN-4 monitoring well (Snæbjörnsdóttir et al., 2017, 2018). The

346   initially dissolved calcite tends to precipitate from this fluid as its pH increases in

347   response to basalt dissolution. Due to the injection of carbon dioxide, more calcite

348   precipitates in this system than it initially dissolved (Matter et al., 2016; Snæbjörnsdóttir

349   et al., 2018). Such carbonate minerals likely tend to preferentially incorporate light Mg

350   into their structure. For example, Mavromatis et al. (2014) found that apparent dolomite-

351   pore fluid δ^{26}Mg fractionation factors were -2.6 ‰, a value similar to that reported by

352   Higgins and Schrag (2010). Numerous other studies have observed the preferential

353   incorporation of light Mg in Mg-bearing carbonates (Galy et al., 2002; Buhl et al., 2007;

354   Hippler et al., 2009; Immenhauser et al., 2010; Wombacher et al., 2011; Li et al., 2012,

355   2015; Pearce et al., 2012; Mavromatis et al., 2012, 2013; Shirokova et al., 2013; Beinlich

356   et al., 2014; Prikryl et al., 2018). Such observations suggests that carbonate precipitation

357   as observed at the CarbFix site would drive the sampled monitoring well to heavier rather

358   than lighter compositions. It seems therefore that carbonate precipitation is not the

359   dominant process controlling the Mg isotope composition of these monitoring well fluids.

360

361   The measured formation water composition requires, therefore, the incorporation

362   of heavy Mg into secondary phases. The calculations reported by Snæbjörnsdóttir et al.

363   (2017, 2018) suggest that Mg-smectites are supersaturated in most of the monitoring

364   fluids collected from the HN-4 monitoring well; the saturation state of the monitoring

365   fluids analyzed in this study with respect to Mg-clay are provided in Table 2. The Mg

366   isotopic compositions of clay minerals tend to be heavier than their co-exisiting fluid

367   phases (Young and Galy, 2004; Tipper et al., 2006; Teng et al., 2007, 2010; Pogge von

368   Strandmann et al., 2008). Similarly, Wimpenny et al. (2010) concluded that the formation

369   of secondary chrysotile, an Mg clay, lead to light Mg release from dissolving basaltic

370   glass and olivine. Ryu et al. (2016) estimated a clay-fluid Mg isotope fractionation factor

371   of 0.54 ‰, for T-O-T clays formed at temperatures from 90 to 250 ºC. Moreover,

372   Wimpenny et al. (2014) measured the brucite-fluid δ^{26}Mg fractionation factor to be

373   0.50‰ at 80 ºC and near to neutral pH. This study argued that this system provided a

374   good analogue to the incorporation of Mg into the octahedral sheets of Mg-rich clay

375   minerals. Note also that ^{26}Mg preferentially adsorbs on the surfaces of kaolinite type

376 minerals, including allophane (Huang et al., 2012; Pogge von Strandmann, 2012;
377 Opfergelt et al., 2014). Thus, both precipitation and adsorption of exchangeable Mg onto
378 clay minerals could lead to the observed pore fluid δ^{26}Mg decrease with time.

379

380   If, to a first approximation, it can be assumed that the Mg isotopic composition of
381 the HN-04 monitoring fluids stem exclusively from the conservative dissolution of
382 basalt[1] having an isotopic composition of δ^{26}Mg$_{basalt}$ = -0.28‰ (Pogge von Strandmann et
383 al., 2008), coupled to the precipitation of a Mg-clay having a Δ^{26}Mg$_{clay\text{-}fluid}$ fractionation
384 factor of 0.50‰ (Wimpenny et al., 2014), the fraction of Mg released to the fluid by the
385 basalt and originally injected into the well with the gas charged fluid that was
386 incorporated into clays can be estimated from mass balance constraints. The Mg
387 concentration of the sampled monitoring well fluids is equal to the sum of contributions
388 from the Mg concentration of the injected gas charged water ($c_{Mg,inject}$), the Mg
389 concentration of the original formation water ($c_{Mg,fw}$), and the change in Mg
390 concentrations due to basalt dissolution ($\Delta c_{Mg,basalt}$) and Mg-clay precipitation ($\Delta c_{Mg,clay}$)
391 such that

392

393      $c_{Mg,measured} = X_{fw}\, c_{Mg,fw} + X_{inject}\, c_{Mg,inject} + \Delta c_{Mg,basalt} - \Delta c_{Mg,clay}$ (1)

394

395 where X_{fw} and X_{inject} are the fraction of formation water and injected water in the
396 collected monitoring well sample, determined by the concentrations of SF$_6$ and SF$_5$CF$_3$
397 tracers in these fluids (Matter et al., 2016) such that $X_{fw} + X_{inject} = 1$. If it can be assumed
398 that the fluids mix and basalt dissolved prior to the precipitation of the Mg-bearing clay,
399 the isotopic composition of the fluid before clay precipitation (δ^{26}Mg$_1$) is given by

400

401 $$\delta^{26}\text{Mg}_1 = \frac{(\delta^{26}\text{Mg}_{fw}\, X_{fw}\, c_{Mg,fw} + \delta^{26}\text{Mg}_{inject}\, X_{inject}\, c_{Mg,inject} + \delta^{26}\text{Mg}_{basalt}\Delta c_{Mg,basalt})}{(X_{fw}\, c_{Mg,fw} + X_{inject}\, c_{Mg,inject} + \Delta c_{Mg,basalt})} \quad (2)$$

402

---

[1] The term conservative dissolution in this regard refers to a process where the dissolution
releases to the fluid Mg having the same isotopic composition as the dissolving rock.

403   where $\delta^{26}Mg_i$ designates the isotopic composition of the indicated source. The Mg

404   isotope compositions of the monitoring well samples can then be determined from an

405   expression of the Rayleigh equation of the form:

406      $$\delta^{26}Mg_{sampled\ fluid} = \delta^{26}Mg_1 - f^{\Delta^{26}Mg_{clay-fluid}} \qquad\qquad (3)$$

407

408   where $\delta^{26}Mg_{sampled\ fluid}$ designates the isotopic composition in the sampled monitoring

409   well fluid, $\Delta^{26}Mg_{clay-fluid}$ stands for the indicated isotope fractionation factor, and f,

410   the fraction of the Mg remaining in the fluid following clay mineral precipitation in each

411   sample. Equations (1) to (3) were solved simultaneously to generate the values of f shown

412   in Fig. 4. The values of X_{fw} and X_{inject} in Eqn. (2) required for this calculations were

413   taken from Matter et al. (2016), and values of $\delta^{26}Mg_{inject}$ and $c_{Mg,inject}$ are provided in

414   Tables 1 and 2. Note the $\delta^{26}Mg_{fw}$ X_{fw} $c_{Mg,fw}$ term is negligible compare to the other

415   terms in Eqn. (2) due to the low Mg concentration of the pre-injection formation waters

416   (compare the composition of sample 12KMG01 with the others in Table 2). The

417   calculated fraction of the Mg remaining in solution into clay minerals, as shown in Fig. 4,

418   tends to decrease with time. Calculations suggest that this fraction decreases

419   continuously from 33 to 12 percent with time from February 8, 2012 to June 8, 2014.

420   This behavior contrasts somewhat with the saturation index of Mg clays, which becomes

421   undersaturated in the sampled monitoring fluids when the injected acid fluid first arrive at

422   the monitoring well – see Table 2. It can be seen in Fig. 4 that the distribution of

423   calculated Mg precipitation fractions exhibit a concave distribution consistent with the

424   slowing of clay formation rates with time. Consistent with the very dilute Mg

425   concentrations of the deep well fluid prior to the injection, it seems likely that this

426   fraction would approach zero over the long-term.

427

428   This estimate, however, is likely a minimum estimate as evidence indicates that

429   calcite dissolved into the gas charged injection waters shortly after they arrive in the

430   subsurface (Matter et al., 2016; Snæbjörnsdóttir et al., 2017, 2018). The dissolution of

431   these calcites would likely release some light Mg to the fluid phase. In addition, the

432   dissolution of basaltic glass and olivine has been reported to initially release light Mg to

433   the fluid (Wimpenny et al., 2010). Indeed, mass balance and reactive path calculations

434   reported by Snæbjörnsdóttir et al. (2017, 2018) suggest that more than 95% of the Mg

435   release by dissolving basaltic glass needed to be incorporated into secondary phases to be

436   consistent with the measured dissolved Mg concentration of the HN-04 monitoring well

437   fluids in March 2013. The stable Mg isotope measurements reported here suggest that the

438   bulk of these secondary Mg phases formed following the CarbFix injections were Mg

439   bearing clays (e.g. smectite).

440

441   It should be emphasized, however, that the calculated results shown in Fig. 4 are

442   highly uncertain due to poor understanding of the Mg isotope fractionation factor

443   between Mg clay minerals and the aqueous fluid. For example, Teng et al. (2010)

444   suggested that the $\Delta^{26}Mg_{clay-fluid}$ deduced from the compositions of South Carolina

445   saprolites range from 0.05‰ to -0.4‰. In contrast, Huang et al. (2012) reported that

446     $\Delta^{26}Mg_{clay-fluid}$ based on the compositions of southern Chinese saprolites ranged from -

447   0.94‰ to -1.94‰. Wimpenny et al. (2014), however, concluded that the Huang et al.

448   (2012) observations were more consistent with a $\Delta^{26}Mg_{clay-fluid}$ of -0.57‰. The

449   computed value of *f*, the fraction of the Mg remaining in the fluid following clay mineral

450   precipitation in each sample determined in this study depends strongly on the value

451   chosen for $\Delta^{26}Mg_{clay-fluid}$. A value of $\Delta^{26}Mg_{clay-fluid}$ = -0.40‰ would yield a final *f*

452   value for the June 8, 2014 sample of 0.07, whereas a $\Delta^{26}Mg_{clay-fluid}$ = -1.00‰ would

453   yield a final *f* value for the June 8, 2014 sample of 0.34. Moreover, it should also be

454   noted that at the pH and fluid composition changed (Schott et al., 2016), so too would

455     $\Delta^{26}Mg_{clay-fluid}$. Such changes also would alter the calculated values of *f*. It follows

456   that precise and accurate values of $\Delta^{26}Mg_{clay-fluid}$ are an essential prerequisite to using

457   the compositions the Mg isotopic compositions of minerals and fluids to quantify natural

458   geochemical processes.

459

460   The formation of Mg clays in response to the injection of CO_2 into basalts, as

461   indicated in this study, is detrimental to carbon storage efforts for two main reasons.

462   First, the formation of these Mg-bearing silicates consume divalent Mg that could

463 otherwise be used for the formation of carbonate minerals. Second, Mg-bearing clays are
464 voluminous, such that they consume valuable porosity and could decrease host rock
465 permeability. The formation of these clays, however, will occur at a distance from the
466 injection well, as their precipitation requires sufficient basalt dissolution to increase the
467 fluid pH to at least 7 (Snæbjörnsdóttir et al., 2017). As such their formation will not
468 likely clog flow pathways near the injection well. Nevertheless, their formation at a
469 distance from these wells will limit somewhat the efficiency of carbon storage efforts in
470 basalts. This potential challenge might be overcome by injecting at higher temperatures,
471 where the formation of magnesite rather than Mg-bearing clays might be favored,
472 however, Mg-silicate alteration phases including mixed-layered clays, chlorite, and
473 epidote are common alteration phases in basalts to at least 280 °C (Snæbjörnsdóttir et al.,
474 2018). Nevertheless, the continuous injection of acidic CO_2-charged fluids may lead to a
475 propagating reaction front that would progressively move these clay minerals further
476 away from the injection well.

477

478   **6. Conclusions**

479   The Mg isotope compositions of monitoring well samples collected in this study
480 are lighter than the host basalts that dissolved in response to the injection of gas charged
481 waters into the CarbFix site. This observation is consistent with the consumption of the
482 divalent Mg cations released by basalt dissolution by isotopically heavier Mg clay
483 minerals, rather than carbonate minerals, which tend to favor the incorporation of
484 isotopically light Mg. This conclusion is supported by the fact that Mg-smectites rather
485 than Mg carbonate phases are commonly observed as secondary phases in basalts altered
486 at low temperatures. Such results demonstrate that the Mg isotopic compositions of
487 monitoring well fluids can be used to provide insight into the fate of Mg during
488 subsurface carbon storage efforts.

489

490   The rates at which Mg precipitates as clay minerals appear to be relatively slow;
491 mass balance calculations suggest that smectite is still continuing to precipitate 2 years
492 after the termination of the acid gas injection – calculations suggest that ~12 percent of
493 the Mg released to the fluid by basalt dissolution remains to be precipitated after two

years. This contrasts with calcite, which has demonstrated to precipitate more than 95%
of the injected CO_2 in less than 2 years (Matter et al., 2016). Although Mg clay mineral
precipitation is relatively slow, its precipitation may limit significantly the efficiency of
carbon storage efforts based on the enhanced weathering of mafic or ultramafic rocks
over the long term (Rigopoulos et al., 2018).

7. References

Alfredsson, H. A., Oelkers, E. H., Hardarsson, B. S., Franzson, H., Gunnlaugsson, E., and
Gislason, S.R. (2013) The geology and water chemistry of the Hellisheidi, SW-Iceland carbon
storage site. *Int. J. Greenhouse Gas Cont*. **12,** 399-418.

Alfredsson, H. A., Mesfin, K.G., and Wolff-Boenisch, D. (2016) The syringe sampler: An
inexpensive alternative borehole sampling technique for CO_2-rich fluids during mineral carbon
storage. *Greenhouse Gases: Sci. Tech*. **6,** 167-177.

An, Y.J., and Huang, F. (2014) A review of Mg isotope analytical methods by MC-ICP-MS. *J.
Earth Sci.-China* **25,** 822-840.

Aradóttir, E., Sigurdardóttir, H., Sigfússon, B., and Gunnlaugsson, E. (2011). CarbFix: A CCS
pilot project imitating and accelerating natural CO_2 sequestration. *Greenhouse Gas Sci
Technol*, **1,** 105-118.

Aradóttir, E., and Hjalmarsson, E. (2018) CarbFix – Public engagement and transparency. *Energy
Procedia*, **146,** 115-120

Archer, D. (2005) Fate of fossil fuel CO_2 in geologic time. *J. Geophys. Res.* **110,** C09S05.

Assayag, N., Matter, J., Ader, M., Goldberg, D., and Agrinier, P., 2009. Water–rock interactions
during a CO_2 injection field-test: Implications on host rock dissolution and alteration effects.
Chem. Geol. **265,** 227-235.

535   Bacon, D. H., Ramanathan, R., Schaef, H. T., and McGrail, B. P. (2014) Simulating geologic co-
536   sequestration of carbon dioxide and hydrogen sulfide in a basalt formation. *Int. J. Greenhouse*
537   *Gas Control* **21,** 165-176.

538   Beinlich, A., Mavromatis, V., Austrheim, H., and Oelkers E.H. (2012) Inter-mineral Mg isotope
539   fractionation during hydrothermal ultramafic rock alteration – Implications for the global Mg-
540   cycle. *Earth Planet. Sci. Let*. **392,** 166-76.

541   Black, J.R., Yin, Q.Z., Casey, W.H. (2006) An experimental study of magnesium-isotope
542   fractionation in chlorophyll-a photosynthesis. *Geochim. Cosmochim. Acta* **70,** 4072-4079.

543   Bolou-Bi, E.B., Vigier, N., Brenot, A. and Poszwa, A. (2009) Magnesium isotope compositions
544   of natural reference materials. *Geostand. Geoanal. Res*. **33**, 95-109.

545   Bolou-Bi, E.B., Poszwa, A., Leyval, C., Vigier, N. (2010) Experimental determination of
546   magnesium isotope fractionation during higher plant growth. *Geochim. Cosmochim. Acta* **74**,
547   2523-2537.

548   Bolou-Bi, E.B., Vigier, N., Poszwa, A., Boudot, J.-P., Dambrine, E. (2012) Effects of
549   biogeochemical processes on magnesium isotope variations in a forested catchment in the
550   Vosges Mountains (France). *Geochim. Cosmochim. Acta* **87,** 341–355.

551   Brenot, A., Cloquet, C., Vigier, N., Carignan, J., and France-Lanord, C. (2008) Magnesium
552   isotope systematics of the lithologically varied Moselle river basin, France. *Geochim.*
553   *Cosmochim. Acta* **72,** 5070-5089.

554   Buhl, D., Immenhauser, A., Smeulders, G., Kabiri, L. and Richter, D.K. (2007) Time series
555   δ^{26}Mg analysis in speleothem calcite: Kinetic versus equilibrium fractionation, comparison
556   with other proxies and implications for palaeoclimate research. *Chem. Geol.* **244,** 715-729.

557   Chang, V.T.C., Williams, R.J.P., Makishima, A., Belshawl, N.S. and O'Nions, R.K. (2004) Mg
558   and Ca isotope fractionation during $CaCO_3$ biomineralisation. *Biochem. Biophys. Res. Comm.*
559   **323,** 79-85.

560   Croviser, J.L., Honnorez, J., Britz, B., and Petit, J.-C. (1992) Dissolution of subglacial volcanic
561   glasses from Iceland: Laboratory study and modelling. *Appl. Geochem.,* **7**, Supplement 1, 55-
562   81.

563   Fisher, A. T. (1998) Permeability within basaltic oceanic crust: *Revs. Geophys.* **36,** 143-182.

564   Flaathen, T. K., Gislason, S. R., Oelkers, E. H., and Sveinbjörnsdóttir, Á. E. (2009) Chemical
565   evolution of the Mt. Hekla, Iceland, groundwaters: A natural analogue for CO_2 sequestration
566   in basaltic rocks. *App. Geochem*. **24,** 463-474.

567   Foster, G.L., Pogge von Strandmann, P.A.E., and Rae, J.W.B. (2010) The boron and magnesium
568   isotopic composition of seawater. *Geochemistry Geophysics Geosystems* **11**, Q08015,
569   doi:10.1029/2010GC003201.

570   Galeczka, I., Wolff-Boenisch, D., Oelkers, E. H., and Gislason, S. R. (2014) An experimental
571   study of basaltic glass–H_2O–CO_2 interaction at 22 and 50°C: Implications for subsurface
572   storage of CO_2. *Geochim. Cosmochim. Acta* **126,** 123-145.

573   Galy, A., Bar-Matthews, M., Halicz, L and O'Nions, R. K. (2002) Mg isotopis compostion of
574   carbonate: In sight from speleothem formation. *Earth. Planet. Sci. Let*. **202,** 105-115.

575   Galy, A., Yoffe, O., Janney, P.E., Williams, R.E., Cloquet, C., Alard, O., Halicz, L., Wadwha, A.,
576   Hutchen, I.D., Ramon, E. and Carignan, J. (2003) Magnesium isotopes heterogeneity of the
577   isotopic standard SRM980 and new reference materials for magnesium-isotope-ratio
578   measurements. *J. Anal. At. Spectrom.* **18,** 1352-1356.

Geske, A., Goldstein, R.H., Mavromatis, V, Richter, D.K., Buhl, D., Kluge, T., John, C.M., and Immenhauser, A. (2015) The magnesium isotope ($\delta^{26}Mg$) signature of dolomites. *Geochim. Cosmochim. Acta* **149,** 131–151.

Geske, A., Zorlu, J., Richter, D.K., Buhl, D., Niedermayr, A., and Immenhauser, A. (2012) Impact of diagenesis and low grade metamorphism on isotope ($\delta^{26}Mg$, $\delta^{13}C$, $\delta^{18}O$ and $^{87}Sr/^{86}Sr$) and elemental (Ca, Mg, Mn, Fe and Sr) signatures of Triassic sabkha dolomites. *Chem. Geol.* **332–333,** 45–64.

Gíslason, S. R., Arnorsson, S. and Armannsson, H. (1996) Chemical Weathering of Basalt in Southwest Iceland; Effects of Runoff, Age of Rocks and Vegetative/glacial Cover. *Am. J. Sci*. **296,** 837-907.

Gíslason, S. R., Broecker, W. S., Gunnlaugsson, E., Snæbjörnsdóttir, S. Ó., Mesfin, K. G., Alfredsson, H. A., Aradottir, E. S., Sigfusson, B., Gunnarsson, I., Stute, M., Matter, J. M., Arnarson, M. T., Galeczka, I. M., Guðbrandsson, S., Stockman, G., Wolff-Boenisch, D., Stefansson, A., Ragnheidardottir, E., Faathen, T., Gysi, A. P., Olssen, J., Didriksen, K., Stipp, S., Menez, B., and Oelkers, E. H. (2014) Rapid solubility and mineral storage of CO_2 in basalt. *Energy Procedia* **63**, 4561-4574.

Gíslason, S.R. and Oelkers, E.H. (2003) Mechanism, rates, and consequences of basaltic glass dissolution: II. An experimental study of the dissolution rates of basaltic glass as a function of pH and temperature. *Geochim. Cosmochim. Acta* **67,** 3817-3832.

Gíslason, S. R., and Oelkers, E. H. (2014) Carbon Storage in Basalt. *Science*, **344,** 373-374.

Gíslason, S. R., Wolff-Boenisch, D., Stefansson, A., Oelkers, E. H., Gunnlaugsson, E., Sigurdardottir, H., Sigfusson, B., Broecker, W.S., Matter, J. W., and Stute. M. (2010) Mineral Sequestration of Carbon Dioxide in Basalt: A Pre-injection Overview of the CarbFix project. *Int. J. Greenhouse Gas Cont*. **4,** 537-45.

Gíslason, S. R., Sigurdardóttir, H., Aradóttir, E. S., and Oelkers, E.H. (2018) A brief history of CarbFix: challenges and victories of the project's phase. *Energy Procedia,* **146,** 103-114.

Goldberg, D. and Slagle, A.L. (2009) A global assessment of deep-sea basalt sites for carbon sequestration. En*ergy Procedia* **1**, 3675-3682.

Goldberg, D., Lackner, K., Han, P., and Wang, T. (2013) Co-Location of Air Capture, Subseafloor CO_2 Sequestration, and Energy Production on the Kerguelen Plateau: *Envir. Sci. Tech.* **47**, 7521-7529.

Goldberg, D. S., Takahashi, T., and Slagle, A. L. (2008) Carbon dioxdie sequestration in deep-sea basalt. *PNAS* **105,** 9920-9925.

Goldberg, D. S., Kent, D. V., and Olsen, P. E. (2010) Potential on-shore and off-shore reservoirs for CO_2 sequestration in Central Atlantic magmatic province basalts. *PNAS,* **107,** 1327-1332.

Gudbrandsson, S., Wolff-Boenisch, D., Gislason, S. R., and Oelkers, E. H. (2011) An experimental study of crystalline basalt dissolution from 2 < pH < 11 and temperatures from 5 to 75 °C. *Geochim. Cosmochim. Acta* **75,** 5496-5509.

Gysi, A. P., and Stefánsson, A. (2012) CO_2-water–basalt interaction. Low temperature experiments and implications for CO_2 sequestration into basalts: *Geochim. Cosmochim. Acta* **81,**129-152.

Harris, R. N., and Chapman, D. S. (2004) Deep-seated oceanic heat flux, heat deficits and hydrothermal circulation, Cambridge, Cambridge University Press, Hydrogeology of the Oceanic Lithosphere.

623 Higgins, J.A. and Schrag, D.P. (2010) Constraining magnesium cycling in marine sediments
624   using magnesium isotopes. *Geochim. Cosmochim. Acta* **74**, 5039-5053.

625 Hin, R.C., Coath, C.D., Carter, P.J., Nimmo, F., Lai, Y.-L., Pogge von Strandmann, P.A.E.,
626   Willbold, M., Leinhardt, Z.M., Walter, M.J., Elliott, T., (2017) Magnesium isotope evidence
627   that accretional vapour loss shapes planetary compositions. *Nature* **549,** 511-515.

628 Hippler, D., Buhl, D., Witbaars, R.m, Richter, D.K., and Immenhauser, A. (2009) Towards a
629   better understanding of magnesium-isotope rations from marine skeletons. *Geochim.*
630   *Cosmochim. Acta* **73**, 6134-6146.

631 Huang K.-J., Teng F.-Z., Wei G.-J., Ma J.-L., and Bao Z.-Y. (2012) Adsorption- and desorption-
632   controlled magnesium isotope fractionation during extreme weathering of basalt in Hainan
633   Island, China. *Earth Planet. Sci. Let.* **359–360,** 73–83.

634 Immenhauser, A., Buhl, D., Richter, D., Niedermayr, A., Riechelmann, D., Dietzel, M., and
635   Schulte, U. (2010) Magnesium-isotope fractionation during low-Mg calcite precipitation in a
636   limestone cave - Field study and experiments. *Geochim. Cosmochim. Acta* **74,** 4346-4364.

637 Khalilabad, M.R., Axelsson, G. and Gislason, S.R. (2008) Aquifer characterization with tracer
638   test technique; permanent CO_2 sequestration into basalt, SW Iceland. *Min. Mag.* **72,** 121-125.

639 Li, W., Chakraborty, S., Beard, B.L., Romanek, C.S., and Johnson, C.M. (2012) Magnesium
640   isotope fractionation during precipitation of inorganic calcite under laboratory conditions.
641   *Earth and Planet. Sci. Let.* **333-334,** 304-316.

642 Li, W., Beard, B.L., Li, C., Xu, H., and Johnson, C.M. (2015) Experimental calibration of Mg
643   isotope fractionation between dolomite and aqueous solution and its geological implications.
644   *Geochim. Cosmochim. Acta* **157,** 164-181.

645 Li, W., Beard, B.L., Li, C., and Johnson, C.M. (2014) Magnesium isotope fractionation between
646   brucite [Mg(OH)$_2$] and Mg aqueous species: Implications for silicate weathering and
647   biogeochemical processes. *Earth and Planet. Sci. Let.* **394,** 82-93.

648 Ling, M.X., Sedaghatpour, F., Teng, F.-Z., Hays, P.D., Strauss, J., Sun, W.D. (2011)
649   Homogeneous magnesium isotopic composition of seawater: an excellent geostandard for Mg
650   isotope analysis. *Rapid. Commun. Mass Sp.* **25**, 2828-2836

651 Liu, P.-P., Teng, F.-Z., Dick, H. J. B., Zhou, M.-F., and Chung S.-L. (2017) Magnesium isotopic
652   composition of the oceanic mantle and oceanic Mg cycling. *Geochim. Cosmochim. Acta* **206,**
653   151-165.

654 Liu, X-M., F-Z. Teng,F.-Z,. Rudnick, R. L., Mcdonough, W. F. and Cummings, M. L. (2014)
655   Massive magnesium depletion and isotope fractionation in weathered basalts. *Geochim.*
656   *Cosmochim. Acta* **135,** 336-349.

657 Maher, K., Johnson, N.C., Jackson, A., Lammers, L.N., Torchinsky, A.B., Weaver, K.L., Bird,
658   D.K., Brown, G.E. (2016) A spatially resolved surface kinetic model for forsterite dissolution.
659   *Geochim. Cosmochim. Acta* **174**, 313-334.

660 Marieni, C., Prikryl, J., Aradottir, E.S., Gunnarsson, I., and Stefansson, A. (2018) Towards
661   'green' geothermal energy: Co-mineralization of carbon and sulphur in geothermal reservoirs.
662   *Int. J. Greenhouse Gas Cont.,* **77,** 96-105.

663 Matter, J. M., Broecker, W., Stute, M., Gislason, S., Oelkers, E., Stefánsson, A., Björnsson, G.
664   (2009) Permanent carbon dioxide storage into basalt: The CarbFix pilot project,
665   Iceland. *Energy Procedia,* **1,** 3641-3646.

666   Matter, J., Takahashi, T., and Goldberg, D. (2007) Experimental evaluation of *in situ* CO_2-water-
667   rock reactions during CO_2 injection in basaltic rocks: Implications for geological CO_2
668   sequestration: *Geochem. Geophy. Geosy.* **6,** 19.

669   Matter, J.M., Stute, M., Snæbjörnsdóttir, S.Ó., Oelkers, E.H., Gislason, S.R., Aradottir, E.S.,
670   Sigfusson, B., Gunnarsson, I., Sigurdardottir, H., Gunnlaugsson, E., Axelsson, G., Alfredsson,
671   H.A., Wolff-Boenisch, D., Mesfin, K., Fernandez de la Reguera Taya, D., Hall, J., Dideriksen,
672   K. and Broecker, W.S. (2016) Rapid carbon mineralization for permanent and safe disposal of
673   anthropogenic carbon dioxide emissions. *Science* **352,** 1312-1314.

674   Mavromatis, V., Gautier, Q., Bosc, O. and Schott, J. (2013) Kinetics of Mg partition and Mg
675   stable isotope fractionation during its incorporation in calcite. *Geochim. Cosmochim. Acta*
676   **114**, 188-203.

677   Mavromatis, V., Meister, P. and Oelkers, E.H. (2014) Using stable Mg isotopes to distinguish
678   dolomite formation mechanisms: A case study from the Peru Margin. *Chem. Geol.* **385**, 84-91.

679   Mavromatis, V., Pearce, C.R., Shirokova, L.S., Bundeleva, I.A., Pokrovsky, O.S., Benezeth, P.
680   and Oelkers, E.H. (2012) Magnesium isotope fractionation during hydrous magnesium
681   carbonate precipitation with and without cyanobacteria. *Geochim. Cosmochim. Acta* **76**, 161-
682   174.

683   McGrail, B. P., Freeman, C. J., Brown, C. F., Sullivan, E. C., White, S. K., Reddy, S., Garber, R.
684   D., Tobin, D., Gilmartin, J. J., and Steffensen, E. J. (2012) Overcoming business model
685   uncertainty in a carbon dioxide capture and sequestration project: Case study at the Boise
686   White Paper Mill. *Int. J. Greenhouse Gas Cont.* **9**, 91-102.

687   McGrail, B. P., Schaef, H. T., Ho, A. M., Chien, Y.-J., Dooley, J. J., and Davidson, C. L. (2006)
688   Potential for carbon dioxide sequestration in flood basalts. *J. Geophys, Res. Solid Earth* **111,**
689   B12201.

690   McGrail, B. P., Spane, F. A., Sullivan, E. C., Bacon, D. H., and Hund, G. (2011) The Wallula
691   basalt sequestration pilot project. *Energy Procedia* **4,** 5653-5660.

692   Norman, M.D., Yaxley, G.M., Bennett, V.C., and Brandon, A.D. (2006) Magnesium isotopic
693   composition of oliving from ther Earth, Mars, Moon and pallasite parent body. *Geophys. Res.*
694   *Let.,* **33,** L15202.

695   Oelkers, E. H. (2001) General kinetic description of multioxide silicate mineral and glass
696   dissolution. *Geochim. Cosmochim. Acta* **65,** 3703-3719.

697   Oelkers, E.H. and Gislason, S.R. (2001) The mechanism, rates and consequences of basaltic glass
698   dissolution: I. An experimental study of the dissolution rates of basaltic glass as a function of
699   aqueous Al, Si and oxalic acid concentration at 25°C and pH = 3 and 11. *Geochim.*
700   *Cosmochim. Acta* **65**, 3671-3681.

701   Oelkers, E. H., Gislason, S. R., and Matter, J. M. (2008) Mineral carbonation of
702   CO_2. *Elements*, **4,** 333-337.

703   Oelkers, E.H., Benning, L.G., Lutz, S., Mavromatis, V., Pearce, C.R. and Plümper, O. (2015) The
704   efficient long-term inhibition of forsterite dissolution by common soil bacteria and fungi at
705   Earth surface conditions. *Geochim. Cosmochim. Acta* **168**, 222-235.

706   Opfergelt, S., Geors, R.B., Burton. K.W., Guicharnaud, R., Siebert, C., Gislason, S. R., and
707   Halliday, A.N. (2011) Seasonal magnesium isotope variations in soil solutions reflecting
708   physico-chemical processes controlling soil weathering fluxes. *Min. Mag.* **75**, 1571.

Opfergelt, S., Burton, K., Georg, R., West, A., Guicharnaud, R., Sigfusson, B., Seibert, C., Gislason, S.R. and Halliday, A. (2014) Magnesium retention on the soil exchange complex controlling Mg isotope variations in soils, soil solutions and vegetation in volcanic soils, Iceland. *Geochim. Cosmochim. Acta* **125,** 110-130.

Olsson, J., Stipp, S. L. S., Makovicky, E., and Gislason, S. R. (2014) Metal scavenging by calcium carbonate at the Eyjafjallajökull volcano: A carbon capture and storage analogue. *Chem. Geol.* **384,** 135-148.

Pearce, C. R., Saldi, G. D., Schott, J., and Oelkers, E. H. (2012) Isotopic fractionation during congruent dissolution, precipitation and at equilibrium: Evidence from Mg isotopes. *Geochim. Cosmochim. Acta* **92,** 170-183.

Pogge von Strandmann, P.A.E., Burton, K.W., James, R.H., van Calsteren, P., Gislason, S.R. and Sigfusson, B. (2008) The influence of weathering processes on riverine magnesium isotopes in a basaltic terrain. *Earth Planet Sci. Let.* **276**, 187-197.

Pogge von Strandmann, P.A.E., Opfergelt, S., Lai, Y.-J., Sugfusson, B., Gislason. S.R. and Burton, K.W. (2011) Variations of Li and Mg isotope ratios in bulk chondrites and mantle xenoliths. *Geochim. Cosmochim. Acta* **75,** 5247–5268.

Pogge von Strandmann, P.A.E., Elliott, T., Marschall, H. R., Coath, C., Lai, Y.-J., Jeffcoate, A. B., and Ioanoc, D. A. (2012) Lithium, magnesium and silicon isotope behaviour accompanying weathering in a basaltic soil and pore water profile in Iceland. *Earth Planet. Sci. Let.* **339–340,** 11–23.

Pogge von Strandmann, P. A. E., Forshaw, J., and Schmidt, D. (2014) Modern and Cenozoic records of seawater magnesium from foraminiferal Mg isotopes. *Biogeosciences*, 5155-5168.

Pokharel, R., Gerrits, R., Schuessler, J.A., Floor, G., Gorbushina, A.A., and von Blanckenburg, F. (2017) Mg isotope fractionation during uptake by a rock-inhabiting, model microcolonial fungus Knufia petricola at acidic and neutral pH. *Environ. Sci. Tech.* **51**, 9691-9699.

Prikryl, J., Stefansson, A., and Pearce, C.R. (2018) Tracing olivine carbonation and serpentinization in CO_2-rich fluids via magnesium exchange and isotopic fractionation. *Geochim. Cosmochim. Acta* **243,** 133-148.

Rigopoulos, I., Harrison, A.L., Delimitis, A., Ioannou, I., Efastathiou, A.M., Kyratsi, T., and Oelkers, E.H. (2018) Carbon sequestration via enhanced weathering of peridotes and basalts in seawater. *App. Geochem.* **91,** 197-218.

Rogers, K. L., Neuhoff, P. S., Pedersen, A. K., and Bird, D. K. (2006) CO_2 metasomatism in a basalt-hosted petroleum reservoir, Nuussuaq, West Greenland. *Lithos,* **92**, 55-82.

Rosenbauer, R. J., Thomas, B., Bischoff, J. L., and Palandri, J. (2012) Carbon sequestration via reaction with basaltic rocks: Geochemical modelling and experimental results. *Geochim. Cosmochim. Acta* **89**, 116−133.

Ryu, J-S., Vigier, N., Decarreau, A., Lee, S.-W., Lee, K.-S., Song, H., and Petit, S. (2016) Experimental investigation of Mg isotope fractionation during mineral dissolution and clay formation. *Chem. Geol.* **445,** 135-145.

Saenger, C., and Wang, Z. (2014) Magnesium isotope fractionation in biogenic and abiogenic carbonates: Implications for paleoenvironmental proxies. *Quaternary Sci. Revs.* **90,** 1-21.

Saulnier, S., Rollion-Bard, C., Vigier, N. and Chaussidon, M. (2012) Mg isotope fractionation during calcite precipitation: An experimental study. *Geochim. Cosmochim. Acta* **91,** 75-91.

Schott, J., Mavromatis, V., Fujii, T., Pearce, C.R., and Oelkers, E.H. (2016) The control of carbonate mineral Mg isotope composition by aqueous speciation: Theoretical and experimental modeling. *Chem. Geol.* **445,** 120–134.

Shirokova, L. S., Mavromatis, V., Bundeleva, I.A., Pokrovsky, O.S., Bénézeth, P., Gérard, E., Pearce, C. R., and Oelkers, E.H. (2012) Using Mg Isotopes to trace cyanobacterially mediated magnesium carbonate precipitation in alkaline lakes. *Aquat. Geochem.* **19,** 1-24.

Sigfusson, B., Gislason, S. R., Matter, J. M., Stute, M., Gunnlaugsson, E., Gunnarsson, I., Aradottir, E. S., Sigurdardottir, H., Mesfin, K. G., Alfredsson, H. A., Wolff-Boenisch, D., Arnarson, M. T., and Oelkers, E. H. (2015) Solving the carbon-dioxide buoyancy challenge: The design and field testing of a dissolved CO_2 injection system. *Int. J. Greenhouse Gas Cont.* **37,** 213-219.

Sigfusson, B., Arnarson, M. T., Snæbjörnsdóttir, S.Ó., Karlsdóttir, M. R., Aradottir, E. S., and Gunnarsson, I. (2018) Reducing emissions of carbon dioxide and hydrogen sulphide at Hellishidi power plant in 2014-2017 and the role of CarbFix in achieving the 2040 Iceland climate goals. *Energy Procedia* **146**, 135-145.

Snæbjörnsdóttir, S.Ó., Wiese, F., Fridriksson, T., Ármannsson, H., Einarsson, G.M. and Gislason, S.R. (2014) CO_2 storage potential of basaltic rocks in Iceland and the oceanic ridges. *Energy Procedia* **63**, 4585-4600.

Snæbjörnsdóttir, S.Ó., Oelkers, E.H., Mesfin, K., Aradóttir, E.S., Dideriksen, K., Gunnarsson, I., Gunnlaugsson, E., Matter, J.M., Stute, M. and Gislason, S.R. (2017) The chemistry and saturation states of subsurface fluids during the in situ mineralisation of CO_2 and H_2S at the CarbFix site in SW-Iceland. *Int. J. Greenhouse Gas Cont.* **58,** 87-102.

Snæbjörnsdóttir, S.Ó., Gislason, S.R., Galecka, I.M., and Oelkers, E.H. (2018) Reaction path modelling of in-situ mineralisation of CO_2 at the CarbFix site at Hellishedi, SW-Iceland. . *Geochim. Cosmochim. Acta.* **58,** 87-102.

Snæbjörnsdóttir, S.Ó., Tomasdottir, S., Sigfusson, B., Aradóttir, E.S., Gunnarsson, G., Niemi, A., Basirat, F., Gislason, S.R., Oelkers, E.H., and Franzson, H. (2018) The geology and hydrology ofghe CarbFix2 site, SW-Iceland. *Energy Procedia* **146**, 146-157.

Stefánsson, A., Arnórsson, S., Gunnarsson, I., Kaasalainen, H., and Gunnlaugsson, E., 2011. The geochemistry and sequestration of H_2S into the geothermal system at Hellisheidi, Iceland. *J. Volcan. Geothermal Res.* **202,** 179-188.

Stockmann, G. J., Wolff-Boenisch, D., Gislason, S. R., and Oelkers, E. H. (2011) Do carbonate precipitates affect dissolution kinetics? 1: Basaltic glass. *Chem. Geol.* **284,** 306-316.

Teng, F.-Z., Wadhwa, M., and Helz, R. T. (2007) Investigation of magnesium isotope fractionation during basalt differentiation: Implications for a chondritic composition of the terrestrial mantle. *Earth Planet. Sci. Let.* **261**, 84-92.

Teng, F.-Z., Li, W., Rudnick, R. L., and Gardner, L. R. (2010a) Contrasting lithium and magnesium isotope fractionation during continental weathering. *Earth Planet. Sci. Let.* **300,** 63-71.

Teng, F.-Z. (2017) Magnesium Isotope Geochemistry. *Revs. Min. Geochem.* **82,** 219-287.

Tipper, E., A. Galy, A., Gaillardet, J. Bickle, M., Elderfield H., and Carder, E. (2006a) The magnesium isotope budget of the modern ocean: Constraints from riverine magnesium isotope ratios. *Earth Planet. Sci. Let.* **250**, 241-253.

795 Tipper, E.T., Galy, A. and Bickle, M.J. (2006b) Riverine evidence for a fractionated reservoir of
796   Ca and Mg on the continents: Implications for the oceanic Ca cycle. *Earth Planet. Sci. Let.*
797   **247,** 267-279.

798 Tipper, E.T., Galy, A., and Bickle, M. (2008) Calcium and magnesium isotope systematics in
799   rivers draining the Himalaya-Tibetan-Plateau region: Lithological or fractionation control?
800   *Geochim. Cosmochim. Acta* **72,** 1057-1075.

801 Tipper, E.T., Calmels, D., Gaillardet, J., Louvet, P., Capmas, F., and Dubacq, B. (2012a) Positive
802   correlation between Li and Mg isotope ratios in the river waters of the Mackenzie Basin
803   challenges the interpretation of apparent isotopic fractionation during weathering. *Earth*
804   *Planet. Sci. Let.* **333,** 35-45

805 Tipper, E.T., Lemarchand, E., Hindshaw, R.S., Reynolds, B.C. and Bourdon, B. (2012b) Seasonal
806   sensitivity of weathering processes: Hints from magnesium isotopes in a glacial stream. *Chem.*
807   *Geol.* **312–313,** 80–92.

808 Uhlig, D., Schuessler, J.A., Bouchez, J.L., Dixon, J., and von Blanckenburg, F. (2017)
809   Quantifying nutrient uptake as driver of rock weathering in forest ecosystems by magnesium
810   stable isotopes. *Biogeosciences* **14**, 3111-3128.

811 Van Pham, H., Aagaard, P., and Hellevang, H. (2012) On the potential for CO_2 mineral storage in
812   continental flood basalts - PHREEQC batch and 1D diffusion - reaction simulations:
813   *Geochem. Trans.* **13,** 12.

814 Wimpenny, J., Gíslason, S.R., James, R. H., Gannoun, A., Pogge Von Strandmann, P.A.E., and
815   Burton, K.W. (2010) The behaviour of Li and Mg Isotopes during primary phase dissolution
816   and secondary mineral formation in basalt. *Geochim. Cosmochim. Acta* **74,** 5259-279.

817 Wimpenny, J., Colla, C.A., Yin, Q.Z., Rustad, J.R., Casey, W.H. (2014) Investigating the
818   behaviour of Mg isotopes during the formation of clay minerals. *Geochim. Cosmochim. Acta*
819   **128,** 178–194.

820 Wolff-Boenisch, D., Wenau, S., Gislason, S. R., and Oelkers, E. H. (2011) Dissolution of basalts
821   and peridotite in seawater, in the presence of ligands, and CO_2: Implications for mineral
822   sequestration of carbon dioxide: G*eochim. Cosmochim. Acta* **75,** 5510-5525.

823 Wombacher, F., Eisenhauer, A., Bohm, F., Gussone, N., Regenberg, M., Dullo, W.-Chr., and
824   Ruggeberg, A. (2011) Magnesium stable isotope fractionation in marine biogenic calcite and
825   aragonite. *Geochim. Cosmochim Acta* **75,** 5797-5818.

826 Young, E. D., and Galy, A. (2004) The isotope geochemistry and cosmochemistry of magnesium.
827   *Revs Min. Geochem.* **55,** 197-230.

828

Figure Captions

830

831 Fig. 1. Maps showing location of the study area (a) Map showing active volcanic zones in

832 Iceland: RP = Reykjanes Peninsula, WVZ = Western Volcanic Zone, SISZ = South

833 Iceland Seismic Zone, MVZ = Mid-Iceland Volcanic Zone, EVZ = Eastern Volcanic

834 Zone and NVZ = Northern Volcanic Zone. (b) Map showing location of central

835 volcanoes (dark gray) on Reykjanes Peninsula and associated fissure swarms (gray).

836 (c) Map of the CO_2 injection site in, Hellisheidi, SW-Iceland. The CarbFix wells are

837 shown as labeled gray dots. Mapped bedrock faults are located toward east and are

838 part of the Hengill fissure swarm - after Alfredsson et al. (2013).

839 Fig 2. The temporal evolution of a) pH and b) Mg concentration of fluids collected from

840 the HN-04 monitoring well, located 500 m away from the HN-02 injection well

841 before during and after the injection of gas charged waters at the CarbFix site. The

842 timing of the two injections is indicated by the two blue bars. Data from

843 Snæbjörnsdóttir et al. (2017) and Alfredsson et al. (2013). The reported

844 uncertainties on these analyses were reported to be ±0.02 units on pH and ±3% on

845 the Mg concentration analyses.

846 Fig 3. The temporal evolution of $\delta^{26}Mg$ of fluids collected from the CarbFix site. Open

847 diamonds illustrate the compositions of shallow wells prior to the injection, whereas

848 the filled circles represent the composition of monitoring well samples. The dashed

849 horizontal line shows the compositions of the basalts at the CarbFix site whereas the

850 timing of the two injections is indicated by the two blue bars – see text.

851 Fig 4. The temporal evolution of the fraction of Mg released by basalt dissolution that has

852 been incorporated into clay minerals ($f_{Mg, clay}$). Fractions were calculated assuming a

853 closed-system Rayleigh model (see text).

854

855

856
857 Table 1. Summary of measured Mg isotopic compositions of pre-injection shallow well
858 fluids, and post-injection monitoring well fluids collected from HN-04. All isotopic
859 compositions were measured at the HELGES lab, GFZ Potsdam. 2SD refers to twice the
860 standard deviation of n MC-ICP-MS measurements of the same solution. The uncertainty
861 of the presented data (relevant for geological interpretation) is estimated to be 0.10 ‰
862 (2SD) for δ^{26}Mg and 0.06 ‰ (2SD) for δ^{25}Mg based on long-term repeated analyses of
863 samples and references materials – see text.
864

| sample	date (day/month /year)	c_{Mg} (mol kg^{-1}) x 10^{-6}	$\delta^{25}Mg_{DSM3}$ (‰)	2SD	$\delta^{26}Mg_{DSM3}$ (‰)	2SD	n	Well
Post-injection monitoring well samples collected from HN-04								
12KGM08	09/02/2012	36	-0.43	0.05	-0.84	0.09	6	HN-04
12KGM11	16/02/2012	51	-0.45	0.06	-0.88	0.10	4	HN-04
12KGM19	27/02/2012	58	-0.49	0.05	-0.94	0.09	4	HN-04
12KGM25	08/03/2012	86	-0.49	0.05	-0.93	0.02	4	HN-04
12KGM33	26/03/2012	101	-0.48	0.04	-0.94	0.01	4	HN-04
12KGM44	18/04/2012	74	-0.54	0.05	-1.05	0.07	4	HN-04
12KGM49	04/05/2012	36	-0.48	0.06	-0.93	0.12	4	HN-04
12KGM60	30/05/2012	54	-0.52	0.06	-1.01	0.12	4	HN-04
12SOS01	08/06/2012	73	-0.53	0.07	-1.02	0.08	4	HN-04
12SOS09	17/07/2012	64	-0.52	0.07	-0.98	0.10	3	HN-04
12SOS15	31/07/2012	66	-0.57	0.04	-1.1	0.08	4	HN-04
12SOS21	14/08/2012	86	-0.51	0.03	-0.99	0.09	4	HN-04
12SOS28	28/08/2012	79	-0.67	0.06	-1.26	0.07	3	HN-04
12SOS34	24/09/2012	69	-0.57	0.04	-1.11	0.05	3	HN-04
12SOS39	29/10/2012	62	-0.59	0.04	-1.14	0.07	4	HN-04
13SOS01	07/01/2013	42	-0.64	0.07	-1.23	0.06	4	HN-04
13SOS10	16/04/2013	39	-0.69	0.07	-1.31	0.04	3	HN-04
13SOS17	10/06/2013	40	-0.62	0.01	-1.22	0.03	4	HN-04
14SOS11	08/06/2014		-0.69	0.06	-1.34	0.10	4	HN-04
Pre-injection samples taken from indicated shallow well.								
08HAA09	07/08/2008	180	-0.33	0.08	-0.64	0.11	5	HK-25
09HAA18	29/05/2010	175	-0.31	0.03	-0.57	0.06	3	HK-12
10HAA25	02/06/2010	226	-0.35	0.08	-0.69	0.13	3	HK-25
10HAA32	25/06/2010	169	-0.29	0.02	-0.59	0.02	2	HK-13
reference materials								
IAPSO seawater (batch a)			-0.47	0.04	-0.90	0.08	8	
IAPSO seawater (batch b)			-0.45	0.05	-0.88	0.08	4	
IAPSO seawater *mean (batch a & b)*			*-0.46*	*0.04*	*-0.90*	*0.08*	*12*	
seawater (reference value)[a]			*-0.43*	*0.06*	*-0.83*	*0.09*		
Cambridge-1			-1.35	0.06	-2.62	0.10	21	
Cambridge-1 *(reference value)*[a]			-1.34	0.03	-2.61	0.05		

865 [a] Published reference values are from compilations by Pogge von Strandmann et al. (2011), An
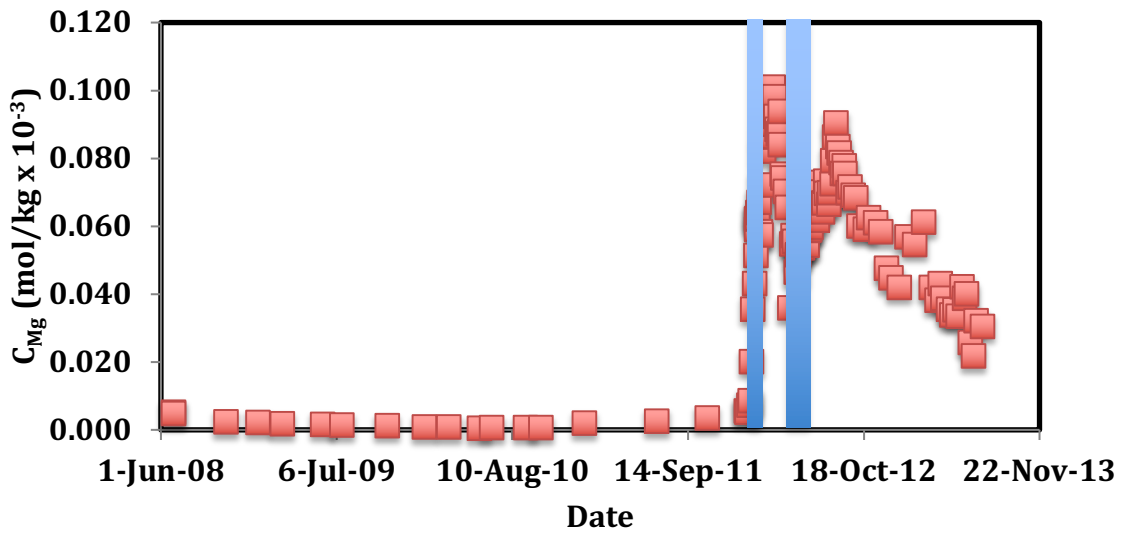866 and Huang (2014), Foster et al. (2010), Ling et al. (2011) and references therein.
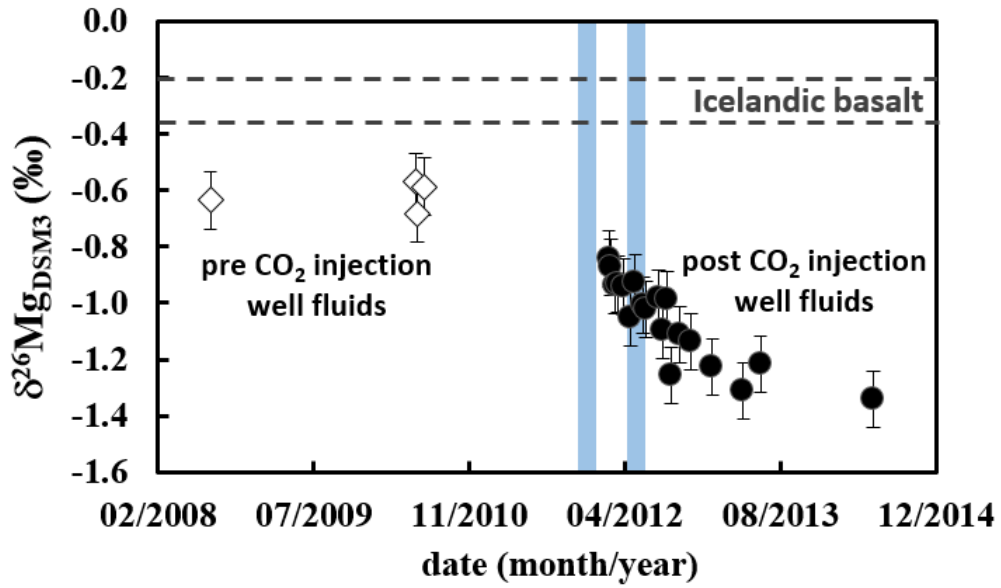867
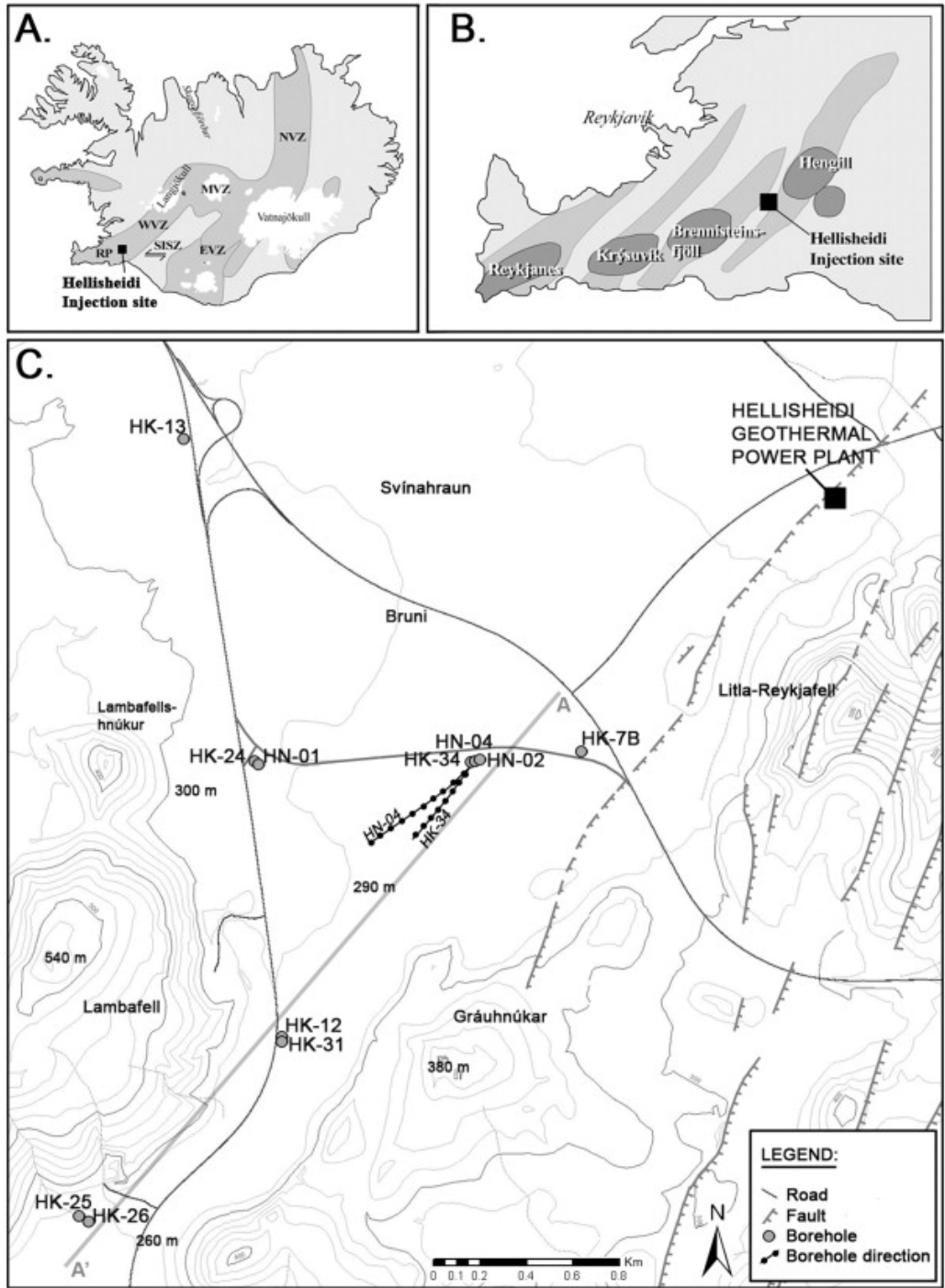
868
869
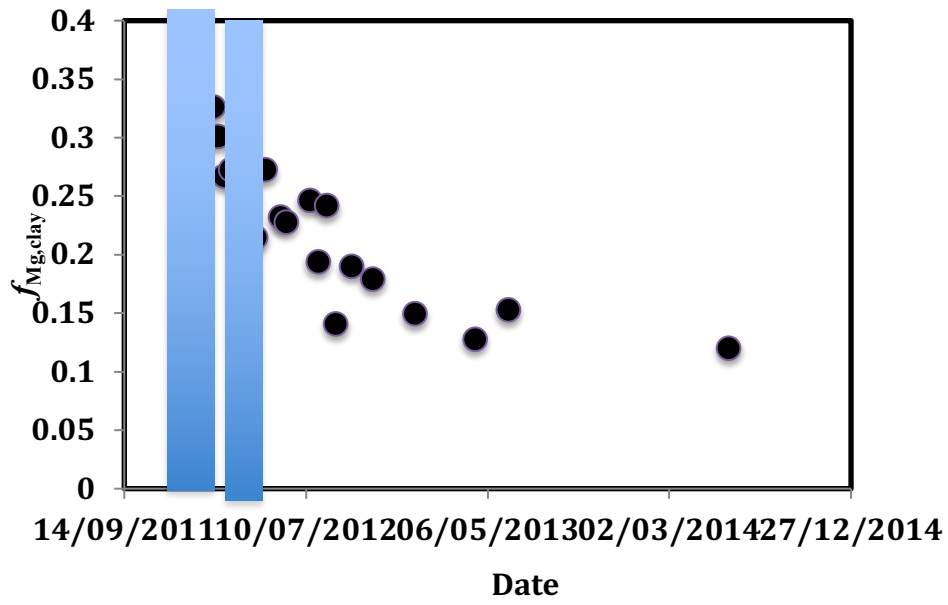870 **Figure 1.**

871

872
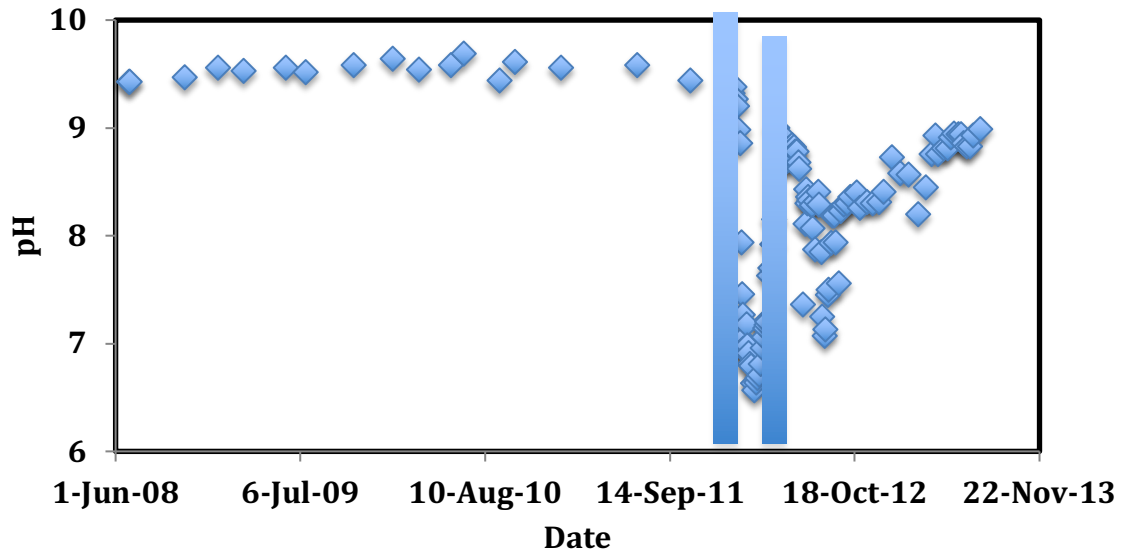
Figure 2.

874

875

876

877 **Figure 3.**

878

879

Figure 4.

881
882
883